Surfactant desorption and scission free energies for cylindrical and spherical micelles from umbrella-sampling molecular dynamics simulations

Boyao Wen [a, b], Bofeng Bai [b] and Ronald G. Larson [a, *]

[a] Department of Chemical Engineering, University of Michigan, Ann Arbor, MI, 48109, United States

[b] State Key Laboratory of Multiphase Flow in Power Engineering, Xi'an Jiaotong University, Xi'an, Shaanxi, 710049, China

* Author to whom correspondence should be addressed. Electronic mail: rlarson@umich.edu; Tel: +1 (734) 936-0772; Fax: +1 (734) 763-0459

Abstract

Hypothesis

The free energies associated with adsorption/desorption of individual surfactants from micelles and the fusion/scission of long micelles can be used to estimate the rate constants for micellar kinetics as functions of surfactant and salt concentration.

Experiments

We compute the escape free energies ΔG_{esc} of surfactant from micelles and the scission free energies ΔG_{sciss} of long micelles from coarse-grained molecular dynamics simulations coupled with umbrella sampling, for micelles of both sodium dodecylsulfate (SDS) in sodium chloride (NaCl) and cetyltrimethylammonium chloride (CTAC) in sodium salicylate (NaSal).

Findings

For spherical micelles, ΔG_{esc} values have maxima at certain aggregation numbers, and at salt-to-surfactant molar concentration ratios R near unity, consistent with experiments. For cylindrical micelles, SDS/NaCl shows a minimum, and CTAC/NaSal a maximum in ΔG_{esc}, both at $R \sim 0.7$, while ΔG_{sciss} of CTAC micelles also peaks at around $R \sim 0.7$ and that of SDS micelles increases monotonically with R. We explain the non-monotonic dependence of escape and scission free energies on R

by a combination of electrostatic screening and the decrease of micelle radius with increasing R. Transitions from predominantly spherical to cylindrical micelles, and between adsorption/desorption and fusion/scission kinetics with changing salt concentration can be inferred from the free energies for CTAC/NaSal.

Keywords: Surfactant micelles; Free energies; Kinetics; Coarse-grained molecular dynamics; Umbrella sampling

1. Introduction

Surfactant solutions self-assemble into a variety of structures, including spherical and wormlike micelles, lamellar sheets, vesicles and lyotropic liquid crystals. Such solutions play a significant role in daily life and many industrial applications and products, such as food, detergents, personal care products, lubricants, and others [1-7]. The diversity of self-assembled structures greatly affects the mechanics, rheology and dynamics of surfactant solutions [8-10]. As the most common and well-studied structures, micelles have sizes and shapes that fluctuate in dynamical equilibrium [11], and whose kinetics are influenced by their structures [12]. The kinetics depend on many factors, such as molecular geometry, surfactant concentration, temperature, and solvent properties including salt type, salt concentration, pH, and so on [13-16]. Understanding how these factors affect the micellar structures and kinetics can contribute to understanding the physics of micelle solutions and provide guidance for formulation of surfactant-containing products.

It is widely accepted that the micellar size changes are dominated by two major types of kinetic processes, which for dilute spherical micelles can be separated by several orders of magnitude in time [11, 17-20]. The so-called “fast” kinetic process is the adsorption/desorption of individual surfactant to and from micelles, which generally has an average time of the order of microseconds [11]. The “slow” kinetics is the micelle fusion/scission whose average time is often on the order of milliseconds to seconds [17-19]. Just above the critical micelle concentration (CMC), surfactants self-assemble into spherical micelles, whose size fluctuations are mainly determined by adsorption/desorption [21]. As surfactant concentration exceeds the so-called “second CMC,” long thread-like or cylindrical micelles become more common, whose size fluctuations are believed to be governed primarily by micelle fusion/scission [22, 23]. Thus, with increasing surfactant concentration, a transition occurs from predominantly adsorption/desorption to predominantly fusion/scission kinetics. In addition, upon a sudden jump in temperature or salt concentration the micelles can find themselves far from equilibrium, leading to a change in the

dominant kinetics [24].

Recent decades have witnessed the development of experimental technologies, theoretical models and molecular simulations for investigating micellar kinetics. Experimental techniques, such as temperature or pressure jump [25, 26], shock tube [27], ultrasonic absorption [28], stopped-flow [29], time-resolved luminescence quenching [30], nuclear magnetic resonance [31] and electron spin resonance [32], have been used to detect the relaxation times of micellar kinetics. On the basis of these experimental techniques, structural parameters, such as the micelle radius, aggregation number, and persistence length, as well as the rheological properties of micellar solutions, can be determined, and are generally consistent with values obtained, or inferred, from our simulation studies presented in what follows. Experimental values for rate constants for micelle kinetics are still scarce, elevating the importance of estimating them computationally. Meanwhile, tracking fast micellar kinetics (e.g., surfactant adsorption/desorption) with very short timescales, or involving multiple components, is still difficult and needs to be further developed. Theoretical modelling of micelle kinetics is a powerful additional tool that has been greatly developed over the last few decades. Aniansson and Wall [33] first derived the fundamental theory of micellar kinetics through stepwise adsorption/desorption of individual surfactants, versions of which have been used to explain the micellar kinetics of various micellar solutions [22, 34-36]. Becker and Döring [37], in particular, applied the equations to the evolution of the micelle size distribution under large deviations from equilibrium [38-41]. These equations, while quite general, require a large number of kinetic coefficients to account for adsorption and desorption rate coefficients for micelles of each size. A method for estimating these from molecular information is needed if the theory is to be applied to real surfactant mixtures.

For long threadlike micelles, Cates [23, 42] determined the dynamics and rheology in response to micelle fusion/scission kinetics only, under the assumptions that the rate of micelle fusion at fixed concentration is independent of micelle length, and that micelle scission occurs at a constant rate per unit length of micelle. These

assumptions reduce the number of rate constants to just two, related to each other by thermodynamics. Shchekin *et al.* [21] avoided these assumptions and adopted the generalized Smoluchowski population balance equation to describe the micelle fusion/scission kinetics. Further, combining the Becker-Döring theory and the general Smoluchowski equations, they obtained a description of both adsorption/desorption and fusion/scission kinetics for spherical and cylindrical micelles and predicted the rates of change in micelle sizes from an initial nonequilibrium size distribution to an equilibrium one [24]. Although the theory of micellar kinetics is thus in principle solved, how to obtain the many parameters of the general theory remains a great challenge, as mentioned above. Since the many rate coefficients are not available experimentally or theoretically, comparisons between such predictions and experimental results have not to our knowledge been attempted so far.

To make further progress, we therefore turn to molecular simulations, from which one can calculate molecular influences on micellar structures and dynamics [43-49], possibly including the rate constants of micellar kinetic theory. Meanwhile, owing to the very different time scales of the fast and slow micellar kinetics, it has become more common to use a combination of simulation methods to model micellar assembly kinetics on multiple scales. For example, using a back-mapping method of coarse-grained to atomistic resolution, Brocos *et al.* [50] combined atomistic and coarse-grained simulations to study surfactant self-assembly in atomic detail. Jusuf and Panagiotopoulos [51] developed a grand canonical Monte Carlo simulation with implicit solvent to speed up the simulation of surfactant micellization. Our group [52-55] has adopted coarse-grained molecular dynamics simulations coupled with umbrella sampling to infer free energy barriers to escape of a surfactant molecule from a spherical micelle and to micelle scission/fusion. Combined with an estimate of a diffusion coefficient, these free energy barriers can be used to infer kinetics of these processes, which can then be compared to experimental study of these processes.

While measurements of surfactant escape and micelle scission free energies and their dependencies on micelle size and salt concentration are experimentally difficult, we show here that enhanced sampling methods in molecular simulations now allow such

properties to be obtained computationally. We use coarse-grained (CG) molecular dynamics (MD) simulations (via the MARTINI forcefield) combined with umbrella sampling to obtain the free energies of adsorption/desorption of a single surfactant (i.e., the escape free energy ΔG_{esc}) and micelle scission (i.e., the scission free energy ΔG_{sciss}) by using the Weighted Histogram Analysis Method (WHAM). We demonstrate non-monotonic dependences of ΔG_{esc} on aggregation number N and salt-to-surfactant concentration ratio R, which depend on the micelle structures (spherical *vs.* cylindrical) and salt types (NaCl *vs.* NaSal). We find that ΔG_{sciss} of SDS cylindrical micelles increases modestly and monotonically with R while that of CTAC cylindrical micelles shows a non-monotonic dependence on R with a maximum at $R \sim 0.7$. Based on these free energies and related theories, we further estimate the escape and breakage times, and discuss the effects of N and R on micellar kinetics.

We treat electrostatics using both a simple cut-off, which is typical for MARTINI CG simulations, and a particle mesh Ewald (PME) summation, and find that for spherical micelles the results are similar, but for cylindrical micelles, although trends are similar, free energies can differ by a factor of two. While this difference has a very large impact on equilibrium micelle lengths and absolute rates of change of micelle size, the ratio of the rate of change by surfactant adsorption/desorption to that by micelle fusion/scission is less sensitive, because both absolute rates are affected similarly by the choice of electrostatic approximation. Here we provide the first practical method to determining from molecular simulations the kinetic coefficients governing the dynamics of micellar size changes, for both adsorption/desorption of individual surfactant molecules and fusion/scission of micelles, at equilibrium or in response to a change of surfactant or salt concentration. While the results obtained need to be confirmed or improved by more accurate atomistic simulations or experiments, the methods developed here provide a crucial next step towards obtaining the kinetic coefficients of Becker-Döring and related models for the micellar kinetics of experimental solutions.

2. Methodology

Simulation setup for spherical/cylindrical micelles. All CG MD simulations were performed using the GROMACS package, version 2019.4 [56]. To reduce the equilibration time and computational cost, we employed the PACKMOL package [57] to generate the preassembled spherical and cylindrical micelles. Then, water beads, hydrated salt ions, including counterions of the surfactant, were dissolved randomly outside the micelles to form the electrically neutral initial simulation systems. Before running an equilibrium simulation, an energy minimization with a steepest-descent algorithm was conducted to keep the force applied on each bead below 1000 $kJ \cdot mol^{-1} \cdot nm^{-2}$. We consider here two simulation systems (SDS/NaCl *vs.* CTAC/NaSal) with spherical or cylindrical micelles, which are common and well-studied in many applications including detergents, body washes and personal care products. Figure 1 shows the typical equilibrated states of SDS/NaCl spherical and cylindrical micelles at T = 300 K after an equilibrium simulation. Boxes are cubic with dimensions around 10 nm for simulations of spherical micelles, and are rectangular for periodic cylindrical micelles with dimensions of around 10-14 nm perpendicular to the micelle and around 18 nm parallel to the micelle. Exact dimensions depend on the simulation, and are given in Table S1 in the *Supplementary Information* (SI). Our goal is to study the effects of surfactant type, aggregation number and salt concentration on the micelle shape and kinetics. The parameter R, which is the ratio of salt to surfactant concentration, describes the effects of salt concentration. Table S2 lists the simulation details and the resulting shapes of micelles after the equilibration simulations. For spherical micelles, the equilibrium micelle changes gradually from spherical to ellipsoidal shape with increasing aggregation number N. As N increases further, the ellipsoidal micelles grow into elongated rod-like or cylindrical micelles. To study the latter, we set up periodic cylindrical micelles without end-caps, that span the box. We found that while, even without salt, a periodic cylindrical SDS micelle can be formed, only after adding NaSal salt is this cylindrical CTAC stable against rapid breakage. The box size chosen for our simulations of SDS and CTAC cylindrical micelles typically corresponds to a concentration of around 0.2 and 0.13 mol/L, respectively. All configurations in this study were visualized with OVITO 3.0.0 [58].

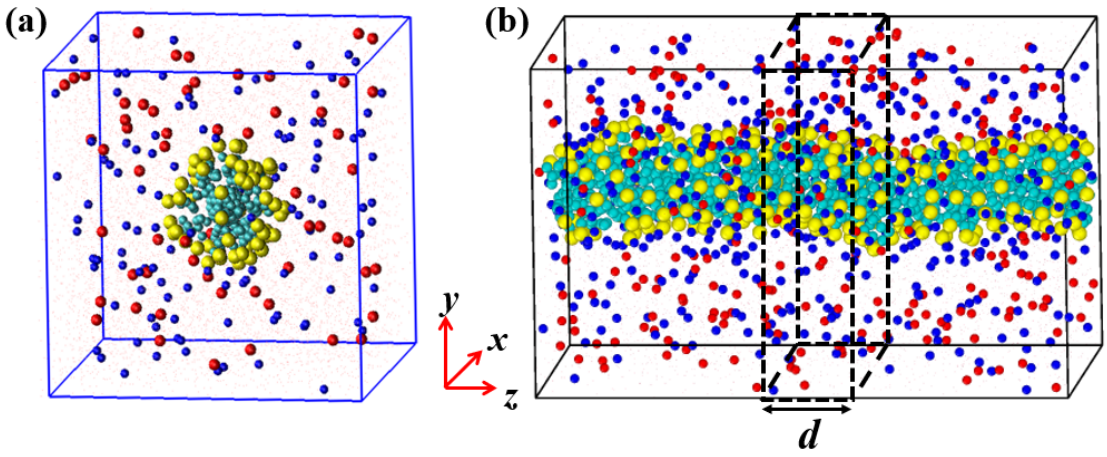

Figure 1. Typical simulation box containing (a) a spherical micelle and (b) a cylindrical micelle of SDS/NaCl at T = 300 K, P = 1 bar. The dashed lines show the scission region (width d = 3 nm) where the biasing potential is applied. The yellow, cyan, blue and red beads represent the surfactant head, surfactant tail, sodium and chloride, beads respectively. Water beads are transparent for clarity.

Force fields. The MARTINI force field [59] with standard coarse-grained water, which has been widely employed to study surfactants [10, 54, 55, 60-62], was used to perform the CG MD simulations of SDS and CTAC surfactant micelles. The coarse-grained representations of surfactants, salts, water and ions used are shown in Figure S1. The bead types of the SDS and CTAC surfactants are drawn from published work [15, 59, 63, 64]. For more details, one can refer to Section 1 of the SI. The short-range nonbonded interactions were implemented using a cut-off distance of 1.2 nm with the bond lengths controlled by LINCS. It is worth noting that the Coulomb potential in the standard MARTINI force field is shifted to zero between 0 and 1.2 nm with permittivity (ε_r) of 15. However, some studies indicate that this shifted cut-off scheme causes unphysical aggregation of multiple MARTINI SDS spherical micelles [49, 65]. As described in previous work of our group [52, 64], we therefore adopted here the PME summation [66] with ε_r = 80 to calculate the electrostatic interactions for both SDS and CTAC micelles, since it does not show micelle aggregation. Since we only consider a single spherical or cylindrical micelle in our simulations, and thus cannot encounter this aggregation phenomenon, we also carry out more limited calculations of free energies with the shifted cut-off for both SDS and CTAC micelles using ε_r = 15. We note that previous work in our group with

the shifted cut-off has given breakage free energies of cylindrical micelles consistent with experiments [55]. While in principle, PME electrostatics should be superior to the shifted cut-off, given the severe approximations used in CG models, including the use of non-polarizable water beads, it is not a priori obvious which method will be more accurate in a given situation. In our simulations, the real-space cutoff of the PME method was 1.2 nm and the Fourier grid spacing was 0.2 nm.

MD Simulation Details. All CG MD simulations were performed in the NPT ensemble. The temperature (300 K) was controlled using a V-rescale thermostat [67], the constant pressure held at 1 bar by using the Parrinello-Rahman barostat [68], both with a time constant of 1 ps. Three-dimensional periodic boundary conditions were applied on the simulation box. To avoid imposing external tension or compression along the axis of the periodic cylindrical micelle, isotropic pressure was imposed using semi-isotropic pressure coupling, which allowed fluctuations of the box dimension parallel to the micelle to be independent of those orthogonal to it. Isotropic pressure coupling was employed in the simulations of spherical micelles. The production simulations were run for 500 ns with a time step of 20 fs.

Umbrella sampling and free energy calculation. To determine the escape free energy ΔG_{esc} of surfactant from micelles and the scission free energy ΔG_{sciss} of cylindrical micelles, we used the umbrella sampling method with a reaction coordinate that can sample sufficiently configurations needed to calculate the potential of mean force (PMF) for each process. For surfactant escaping from micelles, we used as reaction coordinate the center of mass (COM) distance r between the target surfactant molecule and the micelle. For micelle scission/fusion, we adopted as a reaction coordinate the number of surfactant beads (N_d) within a "scission region" (width d = 3nm). A steered "pulling" or "scission" MD simulation was carried out to generate the initial configurations for windows. For each window, a 20 ns umbrella sampling simulation was run to create the output files of reaction-coordinate distributions. Then, we employed the weighed histogram analysis method (WHAM) [69, 70] to obtain the PMF profiles of pulling and scission processes. More details for

the umbrella sampling and free energy calculations are given in Section 2 of the SI.

3. Results and discussion

3.1 Effect of PME on the free energies

Here, we compare the PMF profiles and associated free energies using both PME and cut-off scheme under typical cases, as shown in Figure 2. For the SDS spherical micelle with $N = 60$ at $R = 0$, the height of the change in the PMF gives the surfactant escape free energy ΔG_{esc}. The value of ΔG_{esc} obtained using PME (~ 9.9 kT) is slightly smaller than that obtained using the shifted cut-off (~ 10.5 kT) [52] owing to the long-range electrostatic interactions. Also, inclusion of PME shifts the PMF profile toward the COM of the micelle, presumably because PME loosens the interactions between the charged head groups. However, for high CTAC surfactant and salt concentrations (e.g., 300 CTAC micelle with $R = 1$), the use of PME leads to a significantly smaller ΔG_{esc} (~ 8.1 kT) and scission free energy ΔG_{sciss} (~ 14.2 kT) of the CTAC cylindrical micelle than for the shifted cut-off. This phenomenon may be due to the stronger repulsive interaction between charged surfactant head beads and the long micelle it is leaving when using PME. This presumably allows surfactants to more easily escape from the micelle and for the cylindrical micelle to be more readily broken. Some studies also suggest that the PME scheme gives a more accurate description of the interactions between charged macromolecules [71-73]. Therefore, we adopted the PME electrostatics with $\varepsilon_r = 80$ in most of the following calculations of free energies, but also include some results from the shifted cut-off to check sensitivity to this choice. Additional studies with atomistic forcefields, and comparison with experimental data, will be needed to give reliable quantitative results. Nevertheless, the results presented here do demonstrate the effect of salt-to-surfactant ratio and illustrate the ability of free energy methods to infer details regarding both equilibrium micelle size distributions and rates of micelle size changes.

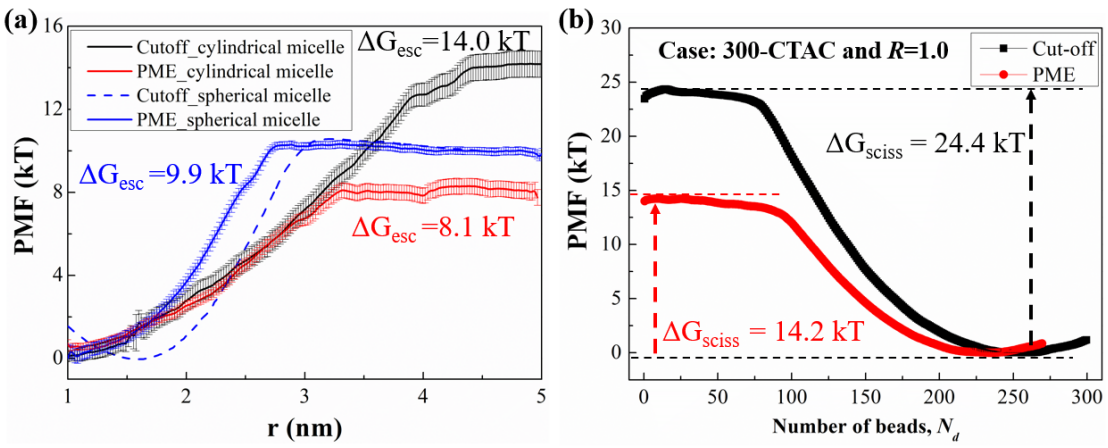

Figure 2. Effects of PME on the PMFs for surfactant escape (a) and for micelle scission (b). Blue lines indicate the result for a spherical micelle with 60 SDS molecules at $R = 0$ while the data of blue dotted line is from ref. [52]. Black and red lines are for a cylindrical micelle with 300 CTAC molecules at $R = 1$. Error bars are the standard deviations. For (b), error bars are comparable to the symbol size and hence not seen.

3.2 Spherical micelles

We computed the radius and eccentricity in shape of both CTAC/NaSal and SDS/NaCl micelles, as described in detail in Section 4.1 of the SI. In brief, the salt NaSal induces greater increases of radius and eccentricity of CTAC spherical micelles with increasing R than for is the case for SDS/NaCl micelles. This is apparently due to stronger electrostatic screening caused by stronger ion adsorption in CTAC/NaSal than is produced by SDS/NaCl micelles.

Escape free energy. To further study the dynamics of spherical micelles, we here calculate the potentials of mean force for the escape of a surfactant from the micelle using umbrella sampling and WHAM. Figure S2 shows the potential of mean force (PMF), which is similar to that shown in Figure 2a above, and representative snapshots of micelles along the reaction coordinate r for pulling a CTAC surfactant from the spherical micelle. The PMF sharply increases as the surfactant crosses the micelle surface from r ~ 1.5 nm to r ~ 3.0 nm and then starts to decrease slightly as r increases above 3.5 nm due to the increasing volume of spherical phase space at increasing r. The escape free energy ΔG_{esc} is defined as the height of PMF profile, from its minimum to its maximum value, which is the free energy barrier that the surfactant must overcome to escape from the micelle. Figure 3 shows the effects of aggregation number N and salt-to-surfactant ratio R on ΔG_{esc} of SDS and CTAC

surfactants pulled from spherical micelles. As in previous work [53], an empirical function given in Figure 3 caption was used to fit the data. As N rises, ΔG_{esc} for a surfactant from the micelle increases at low N and reaches a peak at $N \sim 60$ for SDS and ~ 80 for CTAC. Above this, ΔG_{esc} decreases with N. The maximum in ΔG_{esc} means that the spherical micelle of around this size is the most stable near the CMC and the surfactant has more difficulty escaping from spherical micelles of this size N. The CTAC surfactant has larger ΔG_{esc} than does the SDS surfactant at similar N, owing to the longer hydrophobic tail of the CTAC surfactant. Also, Figure 3b shows that there is a maximum in ΔG_{esc} near $R = 1.0$ for both SDS and CTAC spherical micelles.

The initial increase in ΔG_{esc} is easily understood as the consequence of adsorption of ions with opposite charge onto the micelle surface causing a decrease of the total charge of the micelle, as shown in Figure S7 in the SI; this screens the electrostatic repulsions among surfactant head groups, making it easier to extract them from the micelle. For SDS, the net remaining negative charge on the micelle reaches a minimum near $R \sim 1$ (see Figure S7 in the SI), which then explains the maximum in ΔG_{esc} at this R seen in Figure 3b. For the CTAC micelle, Figure S7 shows that monotonically increasing surface adsorption of salicylate ions induces a *reversal* of the sign of the micelle charge at around $R \sim 1.5$, so that the absolute value of net micelle charge reaches zero and then increases. Thus, pulling a CTA^+ molecule from the negatively charged surface containing an excess of Sal^- should become increasingly more difficult at $R > 1.5$, while the opposite is seen in Figure 3b. This peculiar result could be due to effects of the increase in ionic strength with increasing R, and it is possible that the removal of CTA^+ from the micelle is accompanied by re-arrangements of the surfactant-water interface, such as the re-arrangements of adsorbed Sal^- ions, that are not readily apparent in our averaged profiles. While more detailed examination of the response of the micellar interface to the removal of a CTA^+ might shed light on the issue, these details may be difficult to unravel and sensitive to the forcefield, and so we leave further investigation of this issue to future work. Finally, we note that G_{esc} obtained using cut-off scheme follows a similar trend

with increasing R, but is slightly greater than that obtained using the PME, as shown in Figure 3a and discussed in Section 3.1.

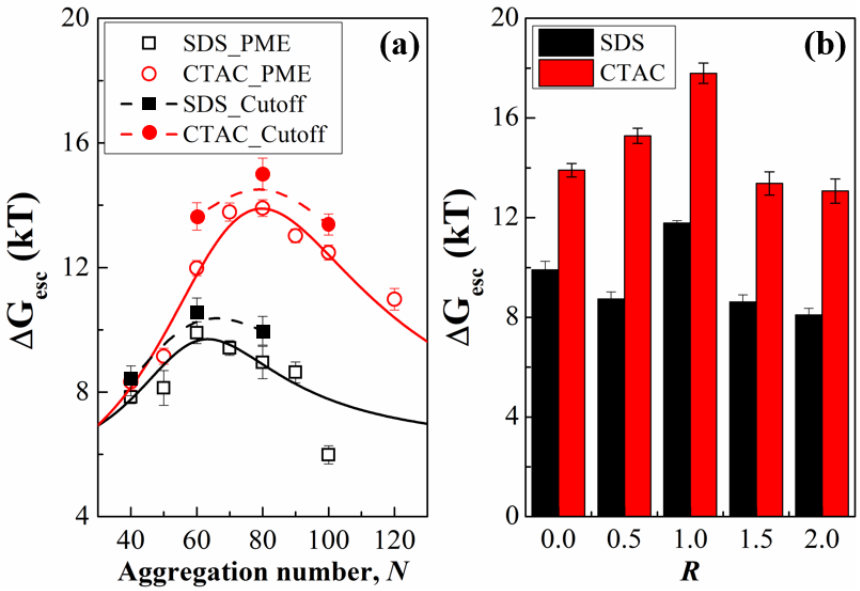

Figure 3. Escape free energies of surfactant from spherical micelles as a function of aggregation number N at $R = 0$ (a) and salt-to-surfactant concentration ratio R (b). The solid lines in (a) are fitted by an empirical equation $f(N) = a + b \times N/(1 + c \times N + d \times N^2)$, and the fitting parameters a, b, c and d are given in Table S3. For (b), spherical micelles with $N = 60$ and 80 are adopted respectively for SDS and CTAC surfactants, both using PME electrostatics. Error bars indicate standard deviations.

Mean first-passage time. Using the PMF profiles of surfactant pulled from the micelles, we can obtain the mean first-passage time for a surfactant to escape from the micelle from the Smoluchowski equation which governs the diffusion of the surfactant molecule in a potential well without inertial effects, given as follows [74]

$$\tau(x, x_f) = \int_x^{x_f} dx' \frac{\exp[W(x')/kT]}{D(x')} \int_{x_0}^{x'} dx'' \exp[-W(x'')/kT] \quad (1)$$

where $\tau(x, x_f)$ is the mean time for a surfactant starting at a position x (near the COM of micelle) to reach the final position x_f. x_0 corresponds to the reflecting boundary for the Smoluchowski equation. In this study, the reaction coordinate r is the same as the position x while x_0 is taken as the smallest value of the reaction coordinate. $D(x')$ is the diffusion coefficient at the position x'. $W(x)$ is the free energy profile (i.e., PMF profile) along x (i.e., along the reaction coordinate r). Since the effects of the diffusion coefficient on the mean first-passage time are far less significant than that of free

energy profile, we treat the diffusion coefficient as a constant, namely 7.40×10^{-6} $cm^2 \cdot s^{-1}$ for SDS [52] and 3.81×10^{-6} $cm^2 \cdot s^{-1}$ for CTAC [75], and we do not attempt to obtain the position-dependent diffusion coefficient.

The resulting mean first-passage time for a surfactant to transfer from the micelle to the bulk phase is shown in Figure 4a. As discussed earlier, PMF profiles are maximum at a distance r of about 3.0 nm away from the COM of the micelle. Beyond this distance, the mean first-passage time profile levels off. Therefore, in this study, the escape time is defined as the mean time for a surfactant to travel from its initial position near the bottom of the PMF well to the position where the PMF reaches a maximum. We find from Figure 4a that the escape times of SDS and CTAC surfactants from a micelle with aggregation number N of 60 are around 5.8 μs and 32.3 μs, respectively. The value for SDS is consistent with the results of atomistic simulation [52] and experiments [11], which indicates that the surfactant exchange between micelles and bulk solution dominates the kinetics of size change of spherical micelles.

We next analyze the influence of N and R on the escape time of SDS and CTAC surfactant, as shown in Figure 4b and 4c. With increasing N, the escape time increases at low N and reaches a peak at an N corresponding to the maximum ΔG_{esc}, which in this study, is $N = 60$ for SDS and $N = 80$ for CTAC. As N rises further, the escape time decreases due to the elongation and reduction of stability of the spherical micelle. Compared to SDS, a CTAC surfactant has a longer escape time. Moreover, the escape times of both surfactants show qualitatively similar dependences on R, including a pronounced maximum near $R = 1.0$, although remaining much larger for CTAC than for SDS, as shown by the differing scales of the right and left axes. This means that the salts significantly increase the escape time at $R \sim 1.0$ and induce the formation of more stable spherical micelles, which may due to the stronger electrostatic screening by the adsorption of ions onto the micelle surface.

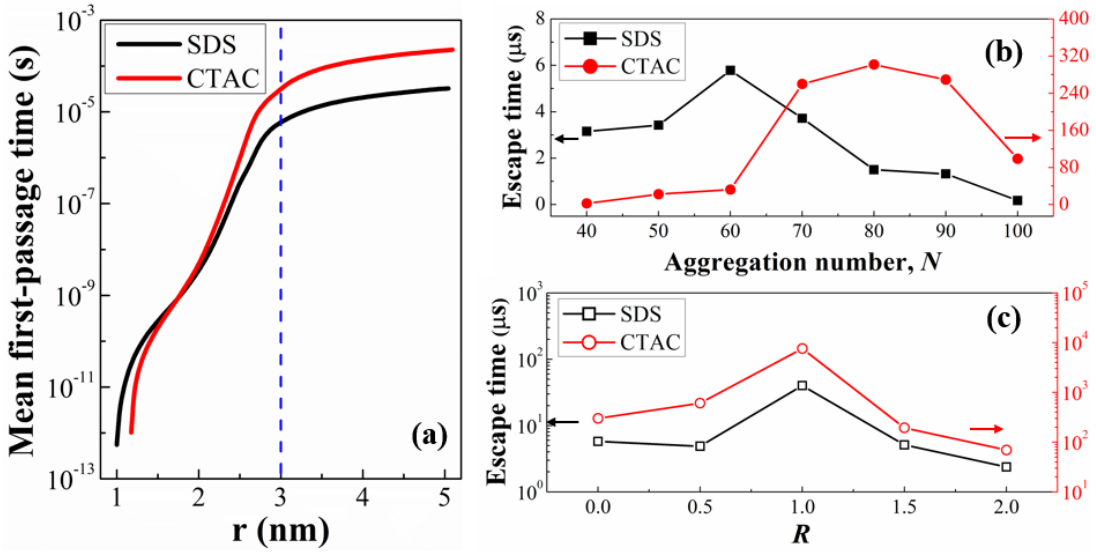

Figure 4. (a) Mean first-passage time for SDS and CTAC surfactants to escape from their spherical micelles at aggregation number N of 60. The blue dotted line represents the position ($r \sim$ 3.0 nm) of maximum PMF values, which is adopted to calculate the escape times as functions of N for $R = 0$ (b) and as functions of R for spherical micelles of optimal size (c).

3.3 Cylindrical micelles

For cylindrical micelles, the strong adsorption of relatively large salicylate ions results in thinner and longer cylindrical CTAC micelles due to the electrostatic screening. Details of this can be found in Section 4.2 (Figure S13) of the SI.

Escape free energy and escape time. As we did for spherical micelles, we here calculate the escape free energy ΔG_{esc} of surfactant from a cylindrical micelle using umbrella sampling and WHAM. Figure 5a shows that ΔG_{esc} is non-monotonic in R, and dependent on the surfactant and ion type. While ΔG_{esc} of SDS from a spherical micelle is maximum at $R \sim 1.0$ (see Figure 3b), for a cylindrical micelle ΔG_{esc} *decreases* to a minimum at $R \sim 0.75$, followed by an increase at higher R. For CTAC micelles, ΔG_{esc} depends similarly on R for both spherical and cylindrical micelles; compare Figure 5a with Figure 3b; both have maxima, which is around 12 kT at $R \sim$ 0.67 for a cylindrical micelle, and around 18 kT at $R \sim 1.0$ for a spherical one. Both for SDS and CTAC cylindrical micelles, the cut-off electrostatics gives greater values of ΔG_{esc} than does the PME electrostatics, although ΔG_{esc} shows a similar dependence on the R. Mandal and Larson showed that the radius of a cylindrical micelle influences ΔG_{esc} [54], suggesting that the nonlinear dependence of ΔG_{esc} on R arises

from a combination of electrostatic screening by adsorbed oppositely charged ions and the dependence of micelle radius on salt concentration. For ΔG_{esc} of a CTAC surfactant from a cylindrical micelle, the adsorption of salicylate ions on the micelle surface screens the electrostatic interaction between surfactant charged head groups making it harder for charged surfactants to escape the micelle, since there is less electrostatic repulsion. This can account for the increase in ΔG_{esc} with R at $R < 1$. If we ignore the effect of micelle radius, we might expect ΔG_{esc} to reach a maximum at $R \sim 1.0$, where the micelle is effectively charge neutral and has smallest electrostatic repulsion between surfactant head groups owing to the strong adsorption of salicylate ions. However, ΔG_{esc} shows a maximum at a smaller $R \sim 0.67$, perhaps because the cylindrical micelle becomes thinner with R increasing, which reduces ΔG_{esc}. Thus, the combination of micelle charge neutralization and reduced micelle radius might explain the shift in the maximum ΔG_{esc} to $R < 1$.

We find much less adsorption of simple sodium ions onto the SDS cylindrical micelle surface at low R than is the case for the hydrophobic salicylate ions onto the CTAC micelle surface. (See Figure S11 in the SI) Thus, the electrostatic screening of ions is weaker for SDS/NaCl micelles and the micelle radius changes less than for CTAC/NaSal micelles. More sodium ions locate outside the micelle surface (See Figure S9(a) in the SI). By integrating the radial dependence of the number density of salt ions around the SDS head group (Figure S10) we find that the fraction of salt ions "bound" to the surfactant head group decreases greatly when the surfactant escapes from the micelle (Table S4). However, the average number of sodium ions bound to the escaped surfactant is maximum at $R = 0.8$ for the cylindrical SDS micelle but not for the spherical micelle (see Table S5). This value of $R = 0.8$ is the same as that for which the peculiar minimum in ΔG_{esc} occurs for the cylindrical SDS micelle but not for the spherical micelle, as mentioned above, suggesting a correlation between the two. With R increasing above 0.8, significant numbers of sodium ions adsorb onto the micelle surface, screening the electrostatic repulsion between head groups, and allowing them to pack more tightly (see Figure S12). This may explain the increase in ΔG_{esc} at higher R, but further work is required to provide a convincing explanation of

the peculiar dependence of ΔG_{esc} on R for cylindrical SDS micelles.

Combining the PMF profiles for surfactant escaping from the cylindrical micelle with Equation 1 for the mean first-passage time, we can obtain the escape time of surfactant from cylindrical micelles, as shown in Figure 5b, assuming that the diffusion coefficients of SDS and CTAC surfactants are the same as those used for spherical micelle. For CTAC cylindrical micelles, a peak in escape time for CTAC surfactant occurs at $R \sim 0.67$, which corresponds to the maximum ΔG_{esc}. This peak is about one order of magnitude larger than those at other R values. For SDS cylindrical micelles, there is a minimum of ΔG_{esc} at $R \sim 0.8$. The escape time for different R for SDS/NaCl is in the range of 0.1-1 μs, which means that the effect of NaCl on the escape time of an SDS surfactant is not as significant as the corresponding effect of NaSal on the CTAC escape time. Compared to the spherical micelles, the much smaller escape times of both SDS and CTAC surfactants from their cylindrical micelles indicates that the surfactant exchange between micelles and the bulk solution is faster for cylindrical than for spherical micelles. We note that the much smaller escape time of surfactant from cylindrical micelles relative to spherical ones is likely due to the stronger electrostatic repulsions between surfactant heads on the micelle surface, arising from the greater aggregation numbers and the smaller surface area-volume ratios of the former.

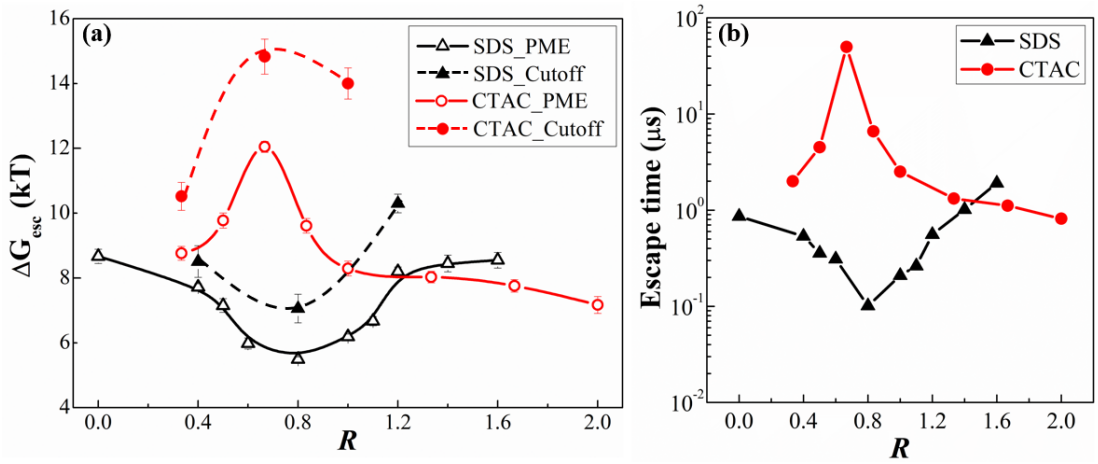

Figure 5. (a) Escape free energies and (b) escape times of SDS and CTAC surfactants from cylindrical micelle as a function of R.

Scission free energy. For long cylindrical micelles, the dynamics of micelle size

change are believed to be controlled by micelle fusion/scission, rather than by adsorption/desorption of individual surfactants. Here, we obtain PMFs and the scission free energies ΔG_{sciss} of periodic cylindrical micelles by umbrella sampling with WHAM, where the reaction coordinate is the number N_d of surfactant beads in the scission region (d = 3 nm), as discussed in the Methodology section. Typical PMFs for SDS and CTAC micelles, with R = 1, are shown in Figure 6a. As N_d decreases, the PMF gradually rises to a plateau that is reached when N_d drops to less than around 100. At large N_d, the PMF has a minimum, which corresponds to the average number of beads in the scission region at equilibrium. ΔG_{sciss} is then the difference between the plateau and the minimum of the PMF. At R = 1, ΔG_{sciss} of the CTAC micelle is larger than that of SDS micelle, mainly owing to the larger micelle radius of the former. The inset of Figure 6a shows that the PMF of micelle scission and its reverse, micelle fusion, are the same, implying that the PMF is reversible, and hence is a thermodynamic quantity, giving an equilibrium free energy of scission.

Figure 6b shows a weak linear increase in ΔG_{sciss} with R for an SDS cylindrical micelle, while for CTAC, ΔG_{sciss} has a local maximum whose magnitude increases and corresponding value of R decreases, when a simple electrostatic cut-off is used as opposed to long-range PME electrostatics. For SDS, since the micelle diameter is nearly independent of R (see Figure S13(b)), we infer that ΔG_{sciss} is mainly governed by electrostatic interactions. As R rises, the weak adsorption of sodium ions onto the micelle surface screens the electrostatic repulsion between surfactant head groups, which presumably produces the weak increase in ΔG_{sciss} with R. For CTAC micelles, ΔG_{sciss} is expected to be strongly affected by both the electrostatics and the micelle radius. At low R (< 0.8), with increasing R, the micelle radius is roughly constant (see Figure S13(b)), so that the strongly increasing electrostatic screening by the adsorption of salicylate ions, induces an increase of ΔG_{sciss}. At high R (> 0.8), the adsorption of salicylate ions on the micelle surface gradually reaches saturation (see Figure S11) and the electrostatic screening begins to saturate. Hence, the reduction of ΔG_{sciss} with increasing R at large R is expected to be dominated by the distinct decrease of micelle radius with increasing R that one finds at large R in Figure S13(b).

While the dependences of PMF on R for the PME and the shifted-cutoff electrostatics are qualitatively similar, the use of PME causes a shift of the peak in ΔG_{sciss} from $R \sim 0.62$ to $R \sim 0.8$ and a significant reduction in height, relative to the curve for the shifted cut-off. The latter change is likely due to the longer-range electrostatic interactions with PME, which makes it easier to break the micelle. Since at low R, the electrostatics has a more important effect on ΔG_{sciss}, the difference of ΔG_{sciss} between PME and shifted cut-off is greater there than at large R, where ΔG_{sciss} is mainly controlled by the micelle radius. Since the adsorption of salicylate ions on micelle surface is saturated at large R, the elongation of cylindrical micelle gradually reaches a limit. The difference in micelle radius obtained using either PME or the cut-off scheme is small; thus the ΔG_{sciss} values for the two cases converge at large R.

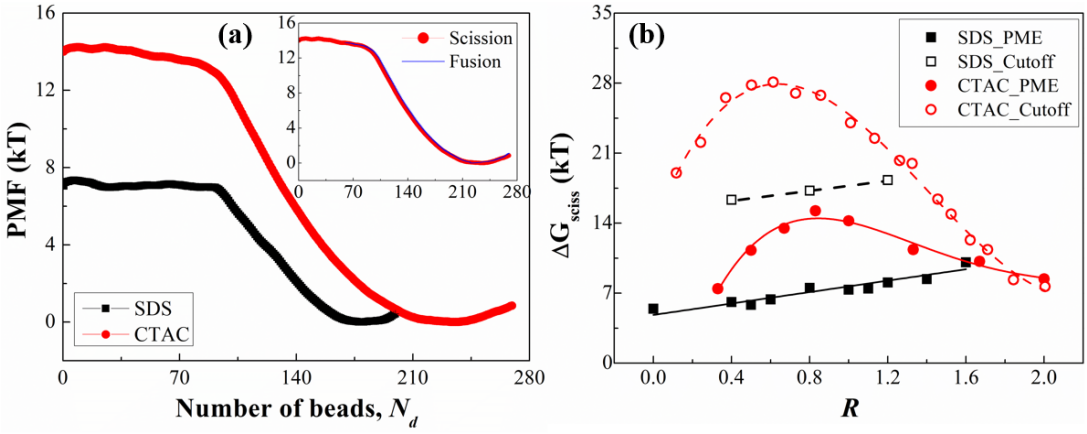

Figure 6. (a) PMFs as functions of the surfactant bead number N in the scission region at R=1 for SDS and CTAC cylindrical micelles. The inset shows the PMFs for scission and fusion processes. Error bars are standard deviations, which are of the order of the symbol size and therefore not visible. (b) Scission free energies of SDS and CTAC cylindrical micelles as functions of R, where for CTAC results using an electrostatic cut-off rather than PME, from ref. [54], are also shown. The surfactant concentration in our work (0.13 mol/L) differs slightly from that in ref. [54] (0.15 mol/L), but this difference should not be significant.

3.4 Micellar equilibrium and kinetics

Spherical micelle CMC. For spherical micelles, we can estimate the mole fraction X_{CMC} of surfactants at the critical micelle concentration (CMC), defined as the concentration at which the number of surfactants in spherical micelles equals the number that remain isolated in solution, by the following equation, which is based on ideal mixing of isolated surfactant molecules and micelles in solvent [13, 52],

$$X_{CMC} = \exp(-\Delta G^0_{esc} / kT) \quad (2)$$

here ΔG^0_{esc} represents the standard state chemical potential for the transfer of a surfactant molecule from solution to a micelle at the CMC, which in this study, we estimate by the surfactant escape free energy ΔG_{esc} determined by umbrella sampling. After obtaining X_{CMC}, we can estimate the CMC in units of molarity, by using CMC = X_{CMC} × 55.5 mol/L. Since ΔG_{esc} depends on micelle aggregation number N as shown in Figure 3(a), we use the fitted maximum values of ΔG_{esc} (~9.7 kT and ~13.9 kT) to estimate the CMC since this represents the most stable, and most probable, micelle size, which is around 63 and 80, for SDS and CTAC micelles, respectively. The corresponding CMC, based on ΔG_{esc} for these sizes, is around 3.4 mM and 0.1 mM for SDS and CTAC micelles, which are smaller by factors of 2.5 and 13, respectively, than the measured CMCs, which are 8.2 mM [76] for SDS and 1.3 mM [77] for CTAC. We attribute these underestimates to inaccuracies ΔG_{esc} resulting from the MARTINI forcefield either with PME (ΔG_{esc} ~ 9.7 kT) or with the shifted cut-off (ΔG_{esc} ~ 10.5 kT) since a PMF from atomistic simulation gives a lower ΔG_{esc} (~ 9.0 kT) [52]. The calculated CMC (~6.8 mM) from atomistic simulation is much closer to the experimental value, suggesting that the deviations in our work are due to the coarse-grained force field. We note in passing that from the dependence of ΔG_{esc} on N, one can estimate the entire micelle size distribution as a function of surfactant concentration, as described by Yuan and Larson [53].

Transition in cylindrical micellar kinetics. For cylindrical micelles, the micellar kinetics may be regulated by the adsorption/desorption (a/d) of individual surfactant molecules or by micelle scission/fusion (f/s), or by a combination of both. To determine which mechanism dominates at a particular salt or surfactant concentration, we compare the rate at which a cylindrical micelle changes its size by roughly a factor two by f/s or by a/d. The rates of a/d and f/s kinetics are controlled by the time constants τ_{esc} and τ_{br}, which are the average escape time of a typical surfactant molecule from the micelle and the breakage time of a cylindrical micelle, respectively. For growth or shrinkage of a micelle of aggregation number N by a/d kinetics, a *net*

addition or subtraction of order ~ N surfactants events must occur. Since τ_{esc} is the mean time for a typical surfactant molecule to escape the micelle, the mean time between single surfactant desorption or adsorption events is $\Delta t_1 = \tau_{esc}/N$. Addition and subtraction events, if taken to be uncorrelated, cancel each other out except for Gaussian drift, and so N^2 such events must occur for the micelle to experience a net change of N surfactants. Thus, the time for micelle growth/shrinkage by stepwise a/d is $\tau_N \sim N^2 \Delta t_1 \sim \tau_{esc} N$.

For scission/fusion of a micelle of size N, the average breakage time τ_{br} is the time for the micelle scission/fusion to roughly halve/double the micelle size, which can be estimated by using the micelle scission energy via the following equation [54]

$$\tau_{br} = \tau_0 \exp(E'_{sci} / kT) \quad (3)$$

where $E'_{sci} = E^0_{sci} - \boldsymbol{F} \cdot d\boldsymbol{r}$ is the effective scission energy under an external tension $\boldsymbol{F}$ along the micelle and τ_0 is a constant that represents the "attempt" time for micelle breakage. Because there is no external force acting on cylindrical micelle in this study, we set F to zero and the effective scission energy then equals the scission free energy ΔG_{sciss} of a cylindrical micelle, as we mentioned before. In ref. [54], the constant τ_0 was found to have a value on the order of ~ 1 ns, which was obtained by calculating from MD simulations the breakage time and effective scission free energy at a series of applied values of external force, needed to accelerate breakage to bring it within the time frame of molecular dynamics simulations.

Assuming that τ_0 and $d\boldsymbol{r}$ are independent of salt concentration, we estimate the constant τ_0 by calculating the breakage time of a cylindrical micelle with low values of R = 0 and 0.33, for SDS and CTAC cylindrical micelles, respectively under several applied values of external force. The external force is applied by decreasing the pressure along the z direction (the micelle axis) while the pressures along the x and y direction are set to 1 bar. Based on Equation 3, the natural logarithm of τ_{br} should be linear with the $\boldsymbol{F}$ (see Figure S14). Extrapolating these linear fits to zero $\boldsymbol{F}$, we can obtain the average breakage time τ_{br} of a cylindrical micelle under no external force. Combined with the scission free energy, the constant τ_0 thus can be determined, which

is about 0.28 ns and 0.65 ns for SDS and CTAC cylindrical micelles, respectively, in our simulations.

We note that the breakage time is inversely proportional to the length (or aggregation number) of the micelle, since each part of a micelle has an equal and independent chance, per unit length, to break. Thus, if we assume that the constant τ_0 is independent of salt concentration and inversely proportional to N we can set $\tau_0 = \tau_{00}/N$ with $\tau_{00} \sim 68$ ns and ~ 195 ns for SDS and CTAC cylindrical micelles respectively to calculate the average breakage time for micelles of different lengths. Actually, this constant is likely affected by the type and concentration of salts, and more precise values deserve to be further investigated, which we leave to our future work. We note that the average aggregation number $\bar{N}$ of a cylindrical micelle is related to the scission free energy ΔG_{sciss} roughly by [23]

$$\bar{N} \approx 2X_{tot}^{1/2} \exp(\Delta G_{sciss} / 2kT) \quad (4)$$

where X_{tot} is the total mole fraction of all surfactant molecules in the solution. (An alternative expression for ideal volumetric mixing entropy produces the same expression except with $\Phi^{1/2}$ replacing $2X_{tot}^{1/2}$, where Φ is the total volume fraction of surfactant [23].)

We now adopt the ratio τ_N/τ_{br}, the ratio of the time for the micelle to double in size by a/d to the time for micelle size doubling via f/s, to estimate which of the two processes is dominant. If the ratio is smaller than unity, the micelle size change will be mainly controlled by the stepwise surfactant adsorption/desorption; otherwise, scission/fusion dominates. Using Figure 5 and $\tau_N \sim \tau_{esc}\bar{N}$ to compute τ_N, and Figure 6b to obtain ΔG_{sciss}, with $\tau_{br} = (\tau_{00}/\bar{N})\exp(\Delta G_{sciss}/kT)$, we plot in Figure 7 the ratio $\tau_N/\tau_{br} = (\tau_{esc}/\tau_{00})\bar{N}^2 \exp(-\Delta G_{sciss}/kT)$ as a function of R for SDS and CTAC cylindrical micelles. To calculate the average aggregation number $\bar{N}$ in this calculation, we use Equation 4 and take mole fractions $X_{tot} = 0.02$ and 0.01 for SDS and CTAC micelles, respectively, giving the values listed in Table S6 in the SI. PME gives unrealistically short cylindrical micelles; i.e., with a maximum no higher than ~400 for CTAC

micelles at R = 0.83, corresponding to micelles only around 25 nm long, and with SDS micelles being too short even to be cylindrical; see Table S6. We therefore also use the shifted cut-off free energies to calculate micelle lengths, and obtain lengths of CTAC micelles ranging from 4 to 14 μm as R increases from 0.33 to 0.50, while SDS micelle length ranges from 0.069 to 0.185 μm, or 69 to 185 nm, for R increasing from 0.4 to 1.2 (see Table S7). These values from the shifted cut-off are more consistent with experiments [78-81]. We took the same constant τ_{00} for both PME and cut-off electrostatics. The ratios τ_N/τ_{br} in Figure 7 derived from these aggregation numbers show a non-monotonic dependence on R, which are different for SDS and CTAC cylindrical micelles. The ratio τ_N/τ_{br} has a minimum at R = 0.8 for SDS cylindrical micelles while that for CTAC cylindrical micelle shows a maximum at R = 0.67, near the value at which the scission free energy has a maximum.

The ratios τ_N/τ_{br} for SDS cylindrical micelles, using either shifted cut-off or PME, are between 0.1 and 10, meaning that the size change of SDS cylindrical micelles is governed by a combination of the adsorption/desorption (a/d) kinetics and micelle fusion/scission (f/s) kinetics. The a/d kinetics plays a dominant role at around $R \sim 0.8$, at which a smaller escape time of an SDS surfactant from a cylindrical micelle occurs apparently due to the binding of sodium ions to the escape surfactant. Both a/d and f/s kinetics are important for SDS cylindrical micelles, because these micelles are relatively short, no longer than 185 nm, and so not drastically different from spherical micelles, for which a/d dynamics is dominant.

For the longer CTAC cylindrical micelles, using either PME or shifted cut-off electrostatics, we find that an increase in NaSal concentration can induce a transition from a mixture of a/d and f/s (at R = 0.33) to predominantly f/s kinetics (at R = 0.67). The higher scission free energies obtained using the electrostatic cut-off method give orders of magnitude longer cylindrical micelles, and therefore much faster scission kinetics, but the trends noted above remain qualitatively the same for both cut-off and PME electrostatics, in particular the transition from a/d to f/s dynamics with increasing salt, up to where the micelle length is maximum. The differences between cut-off and PME electrostatics in the a/d to f/s transitions are not as great as one might

expect, given the exponential dependences of micelle breakage time and surfactant escape time on the breakage and escape free energies. This is because the difference in each of these free energies between cut-off and PME electrostatics are in the same direction, and so compensate each other to some degree. That is, the much slower breakage time implied by cut-off electrostatics, relative to PME, is compensated by the much slower escape time of a surfactant, so that the transition from a/d to f/s is not affected by the treatment of electrostatics as much as might otherwise be the case. The prediction of absolute rates of micelle transitions will be affected to a much great extent, however, which should motivate efforts to carry out free energy simulations for either atomistically resolved molecules, or for improved coarse-grained treatments.

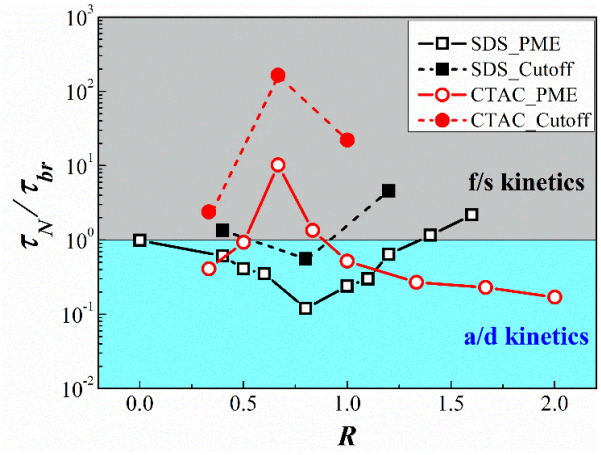

Figure 7. The ratio τ_N/τ_{br} as a function of R for cylindrical micelles with micelle aggregation numbers determined from Eq. 4 and tabulated in Table S6 for PME and cut-off electrostatics. The cyan and gray zone represent the micelle size change dominated by a/d kinetics and f/s kinetics, respectively.

3.5 Consistency of free energy calculations

A cylindrical micelle of a given size can be built up by either fusing together two micelles of half that size, at a rate controlled by ΔG_{sciss}, or by doubling a micelle of half that size by successive addition of individual surfactants, at a rate controlled by ΔG_{esc}. Since the micelle size distribution is set by thermodynamics, there must therefore be an identity relating ΔG_{sciss} to the ΔG_{esc} values for escape of a surfactant from micelles of all sizes up to that of a cylindrical micelle. The detailed derivation of the identity is given in Section 6 of the SI, but the most relevant result is given here:

$$\Delta\mu_{cyl}^{0} \approx \frac{1}{m-1}\sum_{n=2}^{m}\Delta\mu_{n}^{0}=\Delta\bar{\mu}_{n}^{0} \quad (5)$$

where $\Delta\bar{\mu}_{n}^{0}$ is the average value of $\Delta\mu_{n}^{0}$ over the distribution of spherical micelles, and m is the largest aggregation number of a spherical micelle, with larger micelles considered to be "cylindrical." Note that $\Delta\mu_{cyl}^{0}$ and $\Delta\mu_{n}^{0}$, respectively, correspond to the escape free energy ΔG_{esc} from cylindrical and spherical micelles in this work.

Since the above identity requires knowing the escape free energies of all micelle sizes at a given salt concentration, the only case for which we have in this paper obtained the data needed to check this identity is that of SDS spherical and cylindrical micelles with R=0. The average value of the escape free energy for SDS spherical micelles with R=0 is found to be 8.41 kT while the escape free energy of a surfactant from SDS cylindrical micelle with R=0 is 8.67 kT. The near equality of these two values confirms the consistency of the free energies we have obtained by umbrella sampling from MD simulations.

4. Conclusion

We here developed the first practical method for obtaining the free energies and kinetic coefficients of micellar size transitions from molecular simulations. This provides a crucial next step towards supplying the micelle-size-dependent rate constants needed to make the Becker-Döring [37] and related models [24] applicable to predictions of micellar kinetics in experiments. Determination of these rate constants allows us to estimate for the first time the degree to which changes in micelle size occur by adsorption/desorption of individual surfactant molecules or by fusion/scission of micelles. To obtain these rate constants, we applied umbrella sampling simulation methods [52-55] to spherical and cylindrical micelles of sodium dodecylsulfate (SDS) in NaCl solutions and of cetyltrimethylammonium chloride (CTAC) in NaSal solutions for various aggregation numbers (N) and salt-to-surfactant molar ratios (R). We found a non-monotonic dependence of the surfactant escape free energy ΔG_{esc} on N and R, with a peak at N = 60 and 80 for SDS and CTAC,

respectively. At this N, a maximum ΔG_{esc} is achieved at $R = 1$, apparently because the micelle is effectively charge neutralized by salt ions at this value of R. Using the Smoluchowski equation with the computed values of ΔG_{esc}, we obtained the escape time of a surfactant from a micelle as a function of N and R, with results consistent with the literature [11, 52]. In addition, by using ΔG_{esc} and ideal mixture theory, we estimated the CMC of a spherical micelle, which was lower for CTAC surfactants than for SDS ones [77], because of the longer hydrophobic tails of the former.

For cylindrical micelles, our simulations predict non-monotonic dependences of ΔG_{esc} and escape time τ_{esc} of surfactant as functions of R. For CTAC micelles, this non-monotonic behavior is attributed to the electrostatic screening induced by ion adsorption and the reduction of radius with increasing R. The maximum ΔG_{esc} and τ_{esc} occur at $R \sim 0.67$. The scission free energy ΔG_{sciss} of a cylindrical micelle increases slightly with R for SDS micelles, while for CTAC micelles a local maximum in ΔG_{sciss} as a function of R is found, which seems to be set by a combination of electrostatic screening and the salt-dependence of the micelle radius [54]. The use of Particle Mesh Ewald (PME) electrostatics rather than a simple electrostatic cut-off produces a smaller ΔG_{sciss} and a shift of the peak in ΔG_{sciss} from $R \sim 0.62$ [54, 55] to $R \sim 0.8$.

By comparing the scission time estimated from ΔG_{sciss} with the surfactant escape time τ_{esc}, we find that for CTAC/NaSal cylindrical micelles, with increasing R micelle kinetics transition from a mixture of surfactant adsorption/desorption and micelle fusion/scission to predominantly fusion/scission, and then back again, with fusion/scission dominating near $R \sim 0.67$, approximately where the micelle length is greatest. For SDS/NaCl cylindrical micelles, the micelle length is much less sensitive to NaCl concentration, and a reverse transition towards greater dominance of adsorption/desorption is found near $R \sim 0.8$, due to faster surfactant escape from the micelle at this value of R. An identity relating the scission free energy to the escape free energies of a surfactant from spherical micelles of all sizes and from a cylindrical micelle is verified using our calculated free energies.

While the accuracy of the results presented here is limited by our use of coarse-grained force fields, the methods pioneered here can in the future be

implemented with atomistic forcefields, which should improve on their accuracy and allow more quantitative comparisons with experimental results.

CRediT authorship contribution statement

Boyao Wen: Conceptualization, Methodology, Software, Validation, Formal analysis, Investigation, Writing - original draft, Visualization. **Bofeng Bai**: Writing - review & editing, Funding acquisition. **Ronald G. Larson**: Conceptualization, Resources, Writing - review & editing, Supervision, Funding acquisition.

Declaration of Competing Interest

The authors declare that they have no known competing financial interests or personal relationships that could have appeared to influence the work reported in this paper.

Acknowledgement

We are grateful for financial support from the National Science Foundation under grant CBET 1907517. Any opinions, findings, and conclusions or recommendations in this material are those of the authors and do not necessarily reflect the views of NSF. Boyao Wen is supported by the National Natural Science Foundation of China (No.51888103), as well as by the China Scholarship Council. Computational resources and services were provided by Advanced Research Computing at the University of Michigan, Ann Arbor.

Appendix A. Supplementary material

Supplementary material to this article can be found online at https://doi.org/******.

Reference

1. S. Dhakal, R. Sureshkumar, Topology, length scales, and energetics of surfactant micelles, *The Journal of Chemical Physics* 143 (2) (2015) 024905, https://doi.org/10.1063/1.4926422.
2. T. Imae, R. Kamiya, S. Ikeda, Formation of spherical and rod-like micelles of cetyltrimethylammonium bromide in aqueous NaBr solutions, *Journal of Colloid and Interface Science* 108 (1) (1985) 215-225, https://doi.org/10.1016/0021-9797(85)90253-X.
3. F. Lequeux, Structure and rheology of wormlike micelles, *Current Opinion in Colloid & Interface Science* 3 (1) (1996) 341-344, https://doi.org/10.1016/S1359-0294(96)80130-0.
4. D. Danino, Y. Talmon, H. Levy, G. Beinert, R. Zana, Branched threadlike micelles in an aqueous solution of a trimeric surfactant, *Science* 269 (5229) (1995) 1420-1421, https://doi.org/10.1126/science.269.5229.1420.
5. A. S. Poulos, M. Nania, P. Lapham, R. M. Miller, A. J. Smith, H. Tantawy, J. Caragay, J. r. M. Gummel, O. Ces, E. S. Robles, Microfluidic SAXS study of lamellar and multilamellar vesicle phases of linear sodium alkylbenzenesulfonate surfactant with intrinsic isomeric distribution, *Langmuir* 32 (23) (2016) 5852-5861, https://doi.org/10.1021/acs.langmuir.6b01240.
6. Q. Li, J. Wang, N. Lei, M. Yan, X. Chen, X. Yue, Phase behaviours of a cationic surfactant in deep eutectic solvents: from micelles to lyotropic liquid crystals, *Physical Chemistry Chemical Physics* 20 (17) (2018) 12175-12181, https://doi.org/10.1039/C8CP00001H.
7. S. Ezrahi, E. Tuval, A. Aserin, Properties, main applications and perspectives of worm micelles, *Advances in Colloid and Interface Science* 128 (2006) 77-102, https://doi.org/10.1016/j.cis.2006.11.017.
8. J. P. Rothstein, H. Mohammadigoushki, Complex flows of viscoelastic wormlike micelle solutions, *Journal of Non-Newtonian Fluid Mechanics* 285 (2020) 104382, https://doi.org/10.1016/j.jnnfm.2020.104382.
9. J. Larsson, A. Sanchez-Fernandez, A. E. Leung, R. Schweins, B. Wu, T. Nylander, S. Ulvenlund, M. Wahlgren, Molecular structure of maltoside surfactants controls micelle formation and rheological behavior, *Journal of Colloid and Interface Science* 581 (Pt B) (2020) 895-904, https://doi.org/10.1016/j.jcis.2020.08.116.
10. A. Sambasivam, A. V. Sangwai, R. Sureshkumar, Dynamics and scission of rodlike cationic surfactant micelles in shear flow, *Physical Review Letters* 114 (15) (2015) 158302, https://doi.org/10.1103/PhysRevLett.114.158302.
11. R. Zana, *Dynamics of surfactant self-assemblies: micelles, microemulsions, vesicles and lyotropic phases*, CRC Press, 2005.
12. M. Graciani Mdel, A. Rodriguez, V. I. Martin, G. Fernandez, M. L. Moya, Concentration and medium micellar kinetic effects caused by morphological transitions, *Langmuir* 26 (24) (2010) 18659-18668, https://doi.org/10.1021/la102857d.
13. J. N. Israelachvili, *Intermolecular and surface forces*, Academic Press, 2011.
14. M. Amann, L. Willner, J. Stellbrink, A. Radulescu, D. Richter, Studying the concentration dependence of the aggregation number of a micellar model system by SANS, *Soft Matter* 11 (21) (2015) 4208-4217, https://doi.org/10.1039/C5SM00469A.
15. A. V. Sangwai, R. Sureshkumar, Coarse-grained molecular dynamics simulations of the sphere to rod transition in surfactant micelles, *Langmuir* 27 (11) (2011) 6628-6638, https://

doi.org/10.1021/la2006315.
16. V. Patel, N. Dharaiya, D. Ray, V. K. Aswal, P. Bahadur, pH controlled size/shape in CTAB micelles with solubilized polar additives: a viscometry, scattering and spectral evaluation, *Colloids and Surfaces A: Physicochemical and Engineering Aspects* 455 (2014) 67-75, https://doi.org/10.1016/j.colsurfa.2014.04.025.
17. A. Patist, J. R. Kanicky, P. K. Shukla, D. O. Shah, Importance of micellar kinetics in relation to technological processes, *Journal of Colloid and Interface Science* 245 (1) (2002) 1-15, https://doi.org/10.1006/jcis.2001.7955.
18. A. Patist, B. Jha, S. Oh, D. Shah, Importance of micellar relaxation time on detergent properties, *Journal of Surfactants and Detergents* 2 (3) (1999) 317-324, https://doi.org/10.1007/s11743-999-0083-6.
19. S. Oh, D. Shah, Micellar lifetime: Its relevance to various technological processes, *Journal of Dispersion Science and Technology* 15 (3) (1994) 297-316, https://doi.org/10.1080/01932699408943559.
20. R. Leung, D. Shah, Dynamic properties of micellar solutions: I. Effects of short-chain alcohols and polymers on micellar stability, *Journal of Colloid and Interface Science* 113 (2) (1986) 484-499, https://doi.org/10.1016/0021-9797(86)90183-9.
21. A. K. Shchekin, I. A. Babintsev, L. T. Adzhemyan, Full-time kinetics of self-assembly and disassembly in micellar solution via the generalized Smoluchowski equation with fusion and fission of surfactant aggregates, *The Journal of Chemical Physics* 145 (17) (2016) 174105, https://doi.org/10.1063/1.4966233.
22. G. Waton, Kinetics associated with the change of the number density of micelles in solution, *The Journal of Physical Chemistry B* 101 (47) (1997) 9727-9731, https://doi.org/10.1021/jp972480v.
23. M. Cates, S. Candau, Statics and dynamics of worm-like surfactant micelles, *Journal of Physics: Condensed Matter* 2 (33) (1990) 6869, https://doi.org/10.1088/0953-8984/2/33/001.
24. A. K. Shchekin, L. T. Adzhemyan, I. A. Babintsev, N. A. Volkov, Kinetics of aggregation and relaxation in micellar surfactant solutions, *Colloid Journal* 80 (2) (2018) 107-140, https://doi.org/10.1134/S1061933X18020084.
25. N. Muller, Kinetics of micelle dissociation by temperature-jump techniques. Reinterpretation, *The Journal of Physical Chemistry* 76 (21) (1972) 3017-3020, https://doi.org/10.1021/j100665a017.
26. P. Huibers, S. Oh, D. Shah, *Pressure Jump Studies on Micellar Relaxation Time and its Effect on Various Technological Processes*, Surfactant Sci. Series, 1996.
27. J. Lang, C. Tondre, R. Zana, R. Bauer, H. Hoffmann, W. Ulbricht, Chemical relaxation studies of micellar equilibriums, *The Journal of Physical Chemistry* 79 (3) (1975) 276-283, https://doi.org/10.1021/j100570a017.
28. M. Frindi, B. Michels, H. Levy, R. Zana, Alkanediyl-α,ω-bis (dimethylalkylammonium bromide) surfactants. 4. Ultrasonic absorption studies of amphiphile exchange between micelles and bulk phase in aqueous micellar solution, *Langmuir* 10 (4) (1994) 1140-1145, https://doi.org/10.1021/la00016a028.
29. J. Zhang, Z. Ge, X. Jiang, P. Hassan, S. Liu, Stopped-flow kinetic studies of sphere-to-rod transitions of sodium alkyl sulfate micelles induced by hydrotropic salt, *Journal of Colloid and Interface Science* 316 (2) (2007) 796-802, https://doi.org/10.1016/j.jcis.2007.08.067.

30. M. H. Gehlen, F. C. De Schryver, Time-resolved fluorescence quenching in micellar assemblies, *Chemical Reviews* 93 (1) (1993) 199-221, https://doi.org/10.1021/cr00017a010.
31. H. Nery, O. Soederman, D. Canet, H. Walderhaug, B. Lindman, Surfactant dynamics in spherical and nonspherical micelles. A nuclear magnetic resonance study, *The Journal of Physical Chemistry* 90 (22) (1986) 5802-5808, https://doi.org/10.1021/j100280a066.
32. M. A. Bahri, M. Hoebeke, A. Grammenos, L. Delanaye, N. Vandewalle, A. Seret, Investigation of SDS, DTAB and CTAB micelle microviscosities by electron spin resonance, *Colloids and Surfaces A: Physicochemical and Engineering Aspects* 290 (1-3) (2006) 206-212, https://doi.org/10.1016/j.colsurfa.2006.05.021.
33. E. Aniansson, S. Wall, Kinetics of step-wise micelle association, *The Journal of Physical Chemistry* 78 (10) (1974) 1024-1030, https://doi.org/10.1021/j100603a016.
34. E. Aniansson, S. Wall, Kinetics of step-wise micelle association. Correction and improvement, *The Journal of Physical Chemistry* 79 (8) (1975) 857-858, https://doi.org/10.1021/j100575a019.
35. E. Aniansson, S. Wall, M. Almgren, H. Hoffmann, I. Kielmann, W. Ulbricht, R. Zana, J. Lang, C. Tondre, Theory of the kinetics of micellar equilibria and quantitative interpretation of chemical relaxation studies of micellar solutions of ionic surfactants, *The Journal of Physical Chemistry* 80 (9) (1976) 905-922, https://doi.org/10.1021/j100550a001.
36. S. Wall, G. Aniansson, Numerical calculations on the kinetics of stepwise micelle association, *The Journal of Physical Chemistry* 84 (7) (1980) 727-736, https://doi.org/10.1021/j100444a009.
37. R. Becker, W. Döring, Kinetische behandlung der keimbildung in übersättigten dämpfen, *Annalen der Physik* 416 (8) (1935) 719-752, https://doi.org/10.1002/andp.19354160806.
38. M. Kshevetskii, A. Shchekin, F. Kuni, Kinetics of slow relaxation upon the competition between globular and small spherocylindrical micelles, *Colloid Journal* 70 (4) (2008) 455-461, https://doi.org/10.1134/S1061933X0804008X.
39. M. Kshevetskiy, A. Shchekin, Nonlinear kinetics of fast relaxation in solutions with short and lengthy micelles, *The Journal of Chemical Physics* 131 (7) (2009) 074114, https://doi.org/10.1063/1.3204699.
40. I. Babintsev, L. Adzhemyan, A. Shchekin, Micellization and relaxation in solution with spherical micelles via the discrete Becker-Doring equations at different total surfactant concentrations, *The Journal of Chemical Physics* 137 (4) (2012) 044902, https://doi.org/10.1063/1.4737130.
41. I. A. Babintsev, L. Adzhemyan, A. Shchekin, Kinetics of micellisation and relaxation of cylindrical micelles described by the difference Becker-Doring equation, *Soft Matter* 10 (15) (2014) 2619-2631, https://doi.org/10.1039/C3SM52460D.
42. M. Cates, Reptation of living polymers: Dynamics of entangled polymers in the presence of reversible chain-scission reactions, *Macromolecules* 20 (9) (1987) 2289-2296, https://doi.org/10.1021/ma00175a038.
43. R. Pool, P. G. Bolhuis, Prediction of an autocatalytic replication mechanism for micelle formation, *Physical Review Letters* 97 (1) (2006) 018302, https://doi.org/10.1103/PhysRevLett.97.018302.
44. M. Sammalkorpi, M. Karttunen, M. Haataja, Micelle fission through surface instability and formation of an interdigitating stalk, *Journal of the American Chemical Society* 130 (52)

(2008) 17977-17980, https://doi.org/10.1021/ja8077413.
45. J. Gao, S. Li, X. Zhang, W. Wang, Computer simulations of micelle fission, *Physical Chemistry Chemical Physics* 12 (13) (2010) 3219-3228, https://doi.org/10.1039/B918449J.
46. Y. Rharbi, M. Karrouch, P. Richardson, Fusion and fission inhibited by the same mechanism in electrostatically charged surfactant micelles, *Langmuir* 30 (27) (2014) 7947-7952, https://doi.org/10.1021/la501465v.
47. B. Aoun, V. Sharma, E. Pellegrini, S. Mitra, M. Johnson, R. Mukhopadhyay, Structure and dynamics of ionic micelles: MD simulation and neutron scattering study, *The Journal of Physical Chemistry B* 119 (15) (2015) 5079-5086, https://doi.org/10.1021/acs.jpcb.5b00020.
48. A. Jusufi, A. Hynninen, A. Z. Panagiotopoulos, Implicit solvent models for micellization of ionic surfactants, *The Journal of Physical Chemistry B* 112 (44) (2008) 13783-13792, https://doi.org/10.1021/jp8043225.
49. X. Tang, P. H. Koenig, R. G. Larson, Molecular dynamics simulations of sodium dodecyl sulfate micelles in water-the effect of the force field, *The Journal of Physical Chemistry B* 118 (14) (2014) 3864-3880, https://doi.org/10.1021/jp410689m.
50. P. Brocos, P. Mendoza-Espinosa, R. Castillo, J. Mas-Oliva, Á. Pineiro, Multiscale molecular dynamics simulations of micelles: coarse-grain for self-assembly and atomic resolution for finer details, *Soft Matter* 8 (34) (2012) 9005-9014, https://doi.org/10.1039/C2SM25877C.
51. A. Jusufi, A. Z. Panagiotopoulos, Explicit- and implicit-solvent simulations of micellization in surfactant solutions, *Langmuir* 31 (11) (2015) 3283-3292, https://doi.org/10.1021/la502227v.
52. F. Yuan, S. Wang, R. G. Larson, Potentials of mean force and escape times of surfactants from micelles and hydrophobic surfaces using molecular dynamics simulations, *Langmuir* 31 (4) (2015) 1336-1343, https://doi.org/10.1021/la5044393.
53. F. Yuan, R. G. Larson, Multiscale molecular dynamics simulations of model hydrophobically modified ethylene oxide urethane micelles, *The Journal of Physical Chemistry B* 119 (38) (2015) 12540-12551, https://doi.org/10.1021/acs.jpcb.5b04895.
54. T. Mandal, R. G. Larson, Stretch and breakage of wormlike micelles under uniaxial strain: A simulation study and comparison with experimental results, *Langmuir* 34 (42) (2018) 12600-12608, https://doi.org/10.1021/acs.langmuir.8b02421.
55. T. Mandal, P. H. Koenig, R. G. Larson, Nonmonotonic scission and branching free energies as functions of hydrotrope concentration for charged micelles, *Physical Review Letters* 121 (3) (2018) 038001, https://doi.org/10.1103/PhysRevLett.121.038001.
56. M. J. Abraham, T. Murtola, R. Schulz, S. Páll, J. C. Smith, B. Hess, E. Lindahl, GROMACS: High performance molecular simulations through multi-level parallelism from laptops to supercomputers, *SoftwareX* 1 (2015) 19-25, https://doi.org/10.1016/j.softx.2015.06.001.
57. L. Martínez, R. Andrade, E. G. Birgin, J. M. Martínez, PACKMOL: A package for building initial configurations for molecular dynamics simulations, *Journal of Computational Chemistry* 30 (13) (2009) 2157-2164, https://doi.org/10.1002/jcc.21224.
58. A. Stukowski, Visualization and analysis of atomistic simulation data with OVITO–the open visualization tool, *Modelling and Simulation in Materials Science and Engineering* 18 (1) (2009) 015012, https://doi.org/10.1088/0965-0393/18/1/015012.
59. S. J. Marrink, H. J. Risselada, S. Yefimov, D. P. Tieleman, A. H. D. Vries, The MARTINI force field: Coarse grained model for biomolecular simulations, *Journal of Physical*

Chemistry B 111 (27) (2007) 7812-7824, https://doi.org/10.1021/jp071097f.
60. S. Dhakal, R. Sureshkumar, Uniaxial extension of surfactant micelles: Counterion mediated chain stiffening and a mechanism of rupture by flow-induced energy redistribution, *ACS Macro Letters* 5 (1) (2015) 108-111, https://doi.org/10.1021/acsmacrolett.5b00761.
61. S. D. Anogiannakis, P. C. Petris, D. N. Theodorou, Promising route for the development of a computational framework for self-assembly and phase behavior prediction of ionic surfactants using MARTINI, *The Journal of Physical Chemistry B* 124 (3) (2020) 556-567, https://doi.org/10.1021/acs.jpcb.9b09915.
62. P. Wang, S. Pei, M. Wang, Y. Yan, X. Sun, J. Zhang, Study on the transformation from linear to branched wormlike micelles: An insight from molecular dynamics simulation, *Journal of Colloid and Interface Science* 494 (2017) 47-53, https://doi.org/10.1016/j.jcis.2017.01.057.
63. S. Jalili, M. Akhavan, A coarse-grained molecular dynamics simulation of a sodium dodecyl sulfate micelle in aqueous solution, *Colloids and Surfaces A: Physicochemical and Engineering Aspects* 352 (1-3) (2009) 99-102, https://doi.org/10.1016/j.colsurfa.2009.10.007.
64. S. Wang, R. G. Larson, Coarse-grained molecular dynamics simulation of self-assembly and surface adsorption of ionic surfactants using an implicit water model, *Langmuir* 31(4) (2015) 1262-1271, https://doi.org/10.1021/la503700c.
65. J. M. Pires, A. F. Moura, L. C. Freitas, Investigating the spontaneous formation of SDS micelle in aqueous solution using a coarse-grained force field, *Química Nova* 35 (5) (2012) 978-981, http://dx.doi.org/10.1590/S0100-40422012000500021.
66. U. Essmann, L. Perera, M. L. Berkowitz, T. Darden, H. Lee, L. G. Pedersen, A smooth particle mesh Ewald method, *The Journal of Chemical Physics* 103 (19) (1995) 8577-8593, https://doi.org/10.1063/1.470117.
67. G. Bussi, D. Donadio, M. Parrinello, Canonical sampling through velocity rescaling, *The Journal of Chemical Physics* 126 (1) (2007) 014101, https://doi.org/10.1063/1.2408420.
68. M. Parrinello, A. Rahman, Polymorphic transitions in single crystals: A new molecular dynamics method, *Journal of Applied Physics* 52 (12) (1981) 7182-7190, https://doi.org/10.1063/1.328693.
69. S. Kumar, J. M. Rosenberg, D. Bouzida, R. H. Swendsen, P. A. Kollman, The weighted histogram analysis method for free-energy calculations on biomolecules. I. The method, *Journal of Computational Chemistry* 13 (8) (1992) 1011-1021, https://doi.org/10.1002/jcc.540130812.
70. A. Grossfield, WHAM: the weighted histogram analysis method. *version* 2 (9) (2012) 06.
71. C. A. López, A. J. Rzepiela, A. H. De Vries, L. Dijkhuizen, P. H. Hünenberger, S. J. Marrink, Martini coarse-grained force field: extension to carbohydrates, *Journal of Chemical Theory and Computation* 5 (12) (2009) 3195-3210, https://doi.org/10.1021/ct900313w.
72. H. Lee, R. G. Larson, Coarse-grained molecular dynamics studies of the concentration and size dependence of fifth-and seventh-generation PAMAM dendrimers on pore formation in DMPC bilayer, *The Journal of Physical Chemistry B* 112 (26) (2008) 7778-7784, https://doi.org/10.1021/jp802606y.
73. A. J. Rzepiela, D. Sengupta, N. Goga, S. J. Marrink, Membrane poration by antimicrobial peptides combining atomistic and coarse-grained descriptions, *Faraday Discussions* 144 (2010) 431-443, https://doi.org/10.1039/B901615E.
74. S. Izrailev, S. Stepaniants, M. Balsera, Y. Oono, K. Schulten, Molecular dynamics study of

unbinding of the avidin-biotin complex, *Biophysical Journal* 72 (4) (1997) 1568-1581, https://doi.org/10.1016/S0006-3495(97)78804-0.
75. A. M. Khan, S. Khizar, S. A. Khan, S. Ali, A. Shah, M. F. Nazar, F. J. Iftikhar, F. Shah, R. A. Khan, A. R. Khan, Investigation of counterion effects of transition metal cations (Fe^{3+}, Cu^{2+}, Zn^{2+}) on cetrimonium bromide using cyclic voltammetry, *Journal of Molecular Liquids* 313 (2020) 113599, https://doi.org/10.1016/j.molliq.2020.113599.
76. P. H. Elworthy, K. J. Mysels, The surface tension of sodium dodecylsulfate solutions and the phase separation model of micelle formation, *Journal of Colloid and Interface Science* 21 (3) (1966) 331-347, https://doi.org/10.1016/0095-8522(66)90017-1.
77. A. Ralston, D. Eggenberger, H. Harwood, P. D. Brow, The electrical conductivities of long-chain quaternary ammonium chlorides containing hydroxyalkyl groups, *Journal of the American Chemical Society* 69 (9) (1947) 2095-2097, https://doi.org/10.1021/ja01201a004.
78. L. Magid, Z. Li, P. Butler, Flexibility of elongated sodium dodecyl sulfate micelles in aqueous sodium chloride: a small-angle neutron scattering study, *Langmuir* 16 (26) (2000) 10028-10036, https://doi.org/10.1021/la0006216.
79. M. E. Helgeson, T. K. Hodgdon, E. W. Kaler, N. J. Wagner, A systematic study of equilibrium structure, thermodynamics, and rheology of aqueous CTAB/$NaNO_3$ wormlike micelles, *Journal of Colloid and Interface Science* 349 (1) (2010) 1-12, https://doi.org/10.1016/j.jcis.2010.05.045.
80. J. Galvan-Miyoshi, J. Delgado, R. Castillo, Diffusing wave spectroscopy in Maxwellian fluids, *The European Physical Journal. E, Soft Matter* 26 (4) (2008) 369-377, https://doi.org/10.1140/epje/i2007-10335-8.
81. L. Arleth, M. Bergström, J. S. Pedersen, Small-angle neutron scattering study of the growth behavior, flexibility, and intermicellar interactions of wormlike SDS micelles in NaBr aqueous solutions, *Langmuir* 18 (14) (2002) 5343-5353, https://doi.org/10.1021/la015693r.